Article

Macroscopic Poly Schiff Base-Coated Bacteria Cellulose with High Adsorption Performance

Lili Ren [1], Zhihui Yang [1,2], Lei Huang [1], Yingjie He [1], Haiying Wang [1,2,*] and Liyuan Zhang [3,4,*]

[1] School of Metallurgy and Environment, Central South University, Changsha 410083, China; ren_lili@csu.edu.cn (L.R.); yangzh@csu.edu.cn (Z.Y.); znhuanglei@csu.edu.cn (L.H.); yingjiehe@csu.edu.cn (Y.H.)

[2] Chinese National Engineering Research Center for Control and Treatment of Heavy Metal Pollution, Central South University, Changsha 410083, China

[3] Department of Colloid Chemistry, Max Planck Institute of Colloids and Interfaces, 14476 Potsdam-Golm, Germany

[4] Environmental Engineering Research Centre, Department of Civil Engineering, The University of Hong Kong, Pokfulam, Hong Kong, China

* Correspondence: haiyw25@163.com (H.W.); lyzhang@mpikg.mpg.de or zhang_livyl@csu.edu.cn (L.Z.)

check for updates

Abstract: Here, a nanofiber-exfoliated bacteria cellulose aerogel with improved water affinity and high mass transfer was synthesized. Consequently, poly Schiff base can be uniformly coated within the body of bacteria cellulose aerogel without the traditional dispersion treatment. The composite aerogel has adequate mechanical and thermal stability and high mass transfer efficiency. Such an aerogel can serve as a superior adsorbent for flow through adsorption of pollution. Typically, the adsorption capacity towards Cr(VI), Cu(II), Re(VII), Conga red, and Orange G reaches as high as 321.5, 256.4, 153.8, 333.3, and 370.3 mg g^{-1}, respectively. Moreover, the adsorption by this composite aerogel is very fast, such that, for example, at just 2 s, the adsorption is almost finished with Cr(VI) adsorption. Moreover, the composite aerogel exhibits a good adsorption-desorption capability. This research will hopefully shed light on the preparation of bacteria cellulose-derived macroscopic materials powerful in not only environmental areas, but also other related applications.

Keywords: bacteria cellulose; poly Schiff base; chromium; adsorption

1. Introduction

Hexavalent chromium (Cr(VI)), a typical toxic contaminant, is normally discharged by industrial plants, which has strong teratogenicity and carcinogenicity [1–3]. Various technologies have been developed and, among them, adsorption is a popular choice for Cr(VI) owing to its feasibility of operation and cost effectiveness [4–11]. The adsorbent is very important in the adsorption technique, but the current adsorbent mainly suffers from the trade-off between mass transfer and recoverability [12–15]. Typically, high mass transfer requires a good dispersion of adsorbent, but this would decline the recovery efficiency. While high recoverability needs relatively strong noncovalent interaction between adsorbent building blocks, which in turn brings down mass transfer.

Bacteria cellulose (BC), a naturally nanofiber-arranged hydrogel, is a promising candidate adsorbent, exhibiting high mechanical strength and chemical stability [16–23]. Moreover, the highly porous network is of high advantage in boosting the mass transfer within bacteria cellulose. Most recently, a polymer with rich functional groups was adopted to modify the bacteria cellulose to improve the adsorption performance. For example, Jin, X et al. and Wang, J et al. used polyethyleneimine to graft on the bacteria cellulose skeleton for the adsorption of cations (e.g., Cu(II), Pb(II), Hg(II)) [24,25].

Jahan, K et al. and Yang, Z et al. reported the in-situ fabrication of poly(aromatic amine) on bacteria cellulose for effectively separating Cr(VI) from the aqueous solution via reduction and chelation [26,27]. Unfortunately, bacteria cellulose must be dispersed firstly to allow the ultimate interaction between cellulose and polymers [24,27]. This complicates the procedures and moreover weakens the mechanical strength of the final macroscopic product [28]. Moreover, though the batch adsorption performance of these adsorbents were proven to be fine, the dynamic adsorption using macroscopic adsorbent was satisfied to practically purify continuous-flow industrial wastewater, which was scarcely reported.

Here, we report a facile fabrication of bacteria cellulose uniformly coated with poly Schiff base. The pretreatment by sodium silicate was applied first to modify the bacteria cellulose to increase the mass transfer efficiency without breaking the macroscopic structure. As a result, the polymerization of Schiff base proceeded effectively within the body of bacteria cellulose to achieve a uniform coating of polymer. The macroscopic composite monolith exhibits attracting performance in adsorption of Cr(VI) and other typical pollutants in batch and dynamic adsorption tests.

2. Experimental Section

2.1. Materials

The bacterial strain, Gluconacetobacter hansenii (ATCC 53582), was provided by China Center of Industrial Culture Collection. The m-phenylenediamine was purchased from Aladdin Industrial Co., Ltd. (Hangzhou, China). Glutaraldehyde was obtained from Macklin Biochemical Technology Co., Ltd. (Shanghai, China) and other chemical regents were provided from Sinopharm chemical reagent (Shanghai, China).

2.2. Preparation of Porous Bacteria Cellulose/Poly Schiff Base

- Pretreatment

The bacteria cellulose was treated with the solution of alkaline sodium silicate. Then, HCl was added and sodium silicate transformed to NaCl and SiO_2. After the removal of SiO_2 by NaOH, the pretreated bacteria cellulose was freeze-dried and used for polymer coating.

- Polymer Coating

The HCl-protonated m-phenylenediamine was mixed with glutaraldehyde, which formed the oligomer solution due to protonation. The pretreated bacteria cellulose (pBC) was immersed in precursor mixture to absorb the oligomers into matrix of pBC. The poly Schiff base was deposited on cellulose nanofibers by tuning the pH to base. The detail of procedure was given in Supplementary Sections S1.1 and S1.2.

The relative content of poly Schiff base in pBC was estimated according to the following equation:

$$D\% = \frac{W_{product} - W_{BC}}{W_{product}} \times 100\% \tag{1}$$

where the D% is the content percentage of poly Schiff base in the composites, $W_{product}$ is the total mass of composites, W_{BC} is the mass of bacteria cellulose or porous bacteria cellulose.

2.3. Characterization

The attenuated total reflection infrared (ATR) spectrum was recorded on a Nicolet IS50 Fourier transform infrared (FTIR) spectrometer (Thermo Fisher scientific instruments, Waltham, MA, USA) at resolution of 4 cm^{-1} in the range of 400~4000 cm^{-1}. A field emission scanning electron microscopy (SEM, JSM-6360LV, JEOL, Tokyo, Japan) and transmission electron microscopy (TEM, JEOL-2011, Tokyo, Japan) was employed to inspect the morphology. The surface area and porosity of samples were calculated by Brunauer-Emmett-Teller (BET) and Barrett-Joyner-Halenda (BJH) method, respectively

(analysis gas: nitrogen; analysis time: 670 min; thermal delay: 30 s; outgas time: 12 h; bath temperature: 50 °C and outgas temperature: 150 °C) (Autosorb iQ, Quantachrome, Ashland, Virginia, USA) [29]. The crystallographic analysis of aerogels was performed on X-ray diffractometer (XRD) with Cu-Ka radiation (D/Max-RB diffractometer, Rigaku, Tokyo, Japan) from 5~50° by using the dried film of samples. The chemical composition was characterized on a K-Alpha 1063 X-ray photoelectron spectroscope (XPS) with Al Kα X-ray as the excitation source (Thermo Fisher scientific instruments, Waltham, MA, USA).

2.4. Batch Adsorption

A series of adsorption experiments were conducted in the polyethylene vials at 30 °C under 150 rpm rotary shaking. 15 mg adsorbent was accurately weighed and added into the 50 mL Cr(VI) containing solution. The blank assay was carried out under the same condition without any adsorbent simultaneously. The adsorbents were filtrated from the solution by filter paper (pore size ~0.45 μm) after completion of adsorption. The analysis method of Cr(VI) concentration (and other pollutants) was given in Supplementary Section S1.3. Considering the chemical state of Cr, the concentration of Cr(III) can be calculated as $Cr(III) = Cr_{total} - Cr(VI)$. To survey the effect of pH on adsorption capacity, the initial pH of solution was adjusted from 0~6 by 2 M HCl or 2 M NaOH. The adsorption isotherm experiment was implemented at pH 2 for 6 h with the initial Cr(VI) concentration varied from 100~500 mg L^{-1}. For kinetics experiment, Cr(VI) solution with concentration of 400 mg L^{-1} was experienced 1~240 min adsorption at pH 2. The concentration of Cu(II), Re(VII), Conga red, and Orange G solution varied from 50~500 mg L^{-1} for 6 h adsorption to achieve their adsorption isotherm. The Cu(II), Re(VII) and Orange G was adjusted to pH 2 while the Conga red was adjusted to pH 5.5. The adsorption capacity for batch adsorption experiment was calculated as follows:

$$q_t = \frac{C_0 - C_t}{m}V \tag{2}$$

$$q_e = \frac{C_0 - C_e}{m}V \tag{3}$$

where q_t is the adsorption capacity at time t (mg g^{-1}), C_0 is the initial Cr(VI) concentration in solution (mg L^{-1}), C_t is the Cr(VI) concentration in solution at time t (mg L^{-1}), q_e is the equilibrium adsorption capacity (mg g^{-1}), C_e is the equilibrium concentration (mg L^{-1}), m is the weight of adsorbent (g), and V is the volume of solution (L).

2.5. Dynamic Adsorption

For the dynamic adsorption, 0.3 g adsorbent was compressed and squeezed in a glass column with length of 500 mm and ID of 8 mm. 25 mL Cr(VI) solution with concentration of 5~100 mg L^{-1} was adjusted to pH 2 and fed into the top of column using the peristaltic pump with controlling the flow velocity from 28.42~85.26 μL min^{-1} at ambient temperature. The concentration of Cr(VI) (and other pollutant) in effluent was measured by the same method as batch adsorption experiment. For other pollutant, the influent concentration of Cu(II), Re(VII), Conga red and Orange G were 50, 20, 20, and 50 mg L^{-1}, respectively. The Cu(II), Re(VII), and Orange G was adjusted to pH 2 while the Conga red was adjusted to pH 5.5. The removal rate was calculated as follows:

$$R\% = \frac{C_0 - C_a}{C_0} \times 100\% \tag{4}$$

where $R\%$ is the removal rate of effluent, C_0 is the influent concentration of pollutant (mg L^{-1}), C_a is the concentration of pollutant in effluent (mg L^{-1}).

2.6. Desorption and Reusability

The recycle adsorption experiment was tested with 7 successive cycles of dynamic adsorption of Cr(VI). After each cycle, 100 mL 1 M NaOH served as the desorption solution and flowed through the column with 0.3 g adsorbent at flow velocity of 56.84 μL min^{-1}. After being washed by deionized water to neutrality, the adsorbent was freeze-dried for the next cycle.

3. Result and Discussion

3.1. Pretreatment of Bacteria Cellulose

The overview of pathway to fabricate the porous bacteria cellulose/poly Schiff base was described in Scheme 1. Bacteria cellulose was saturated with the sodium silicate solution (alkaline). Then, HCl acid reacted with sodium silicate to produce SiO$_2$ aggregation. The formation of SiO$_2$ could enlarge the inner space of bacteria cellulose and disassemble the large bacteria cellulose fiber bundles into much thinner fibers. The SiO$_2$ was removed by NaOH solution and the pure modified bacteria cellulose was obtained by water rinse and subsequent freeze-drying. After the pretreatment, the bacteria cellulose was still macro-scale monolith. As shown in Figure 1a,b, the smooth surface of pristine bacteria cellulose consisted of compact fibers. In contrast, the pretreated bacteria cellulose had many macroscopic holes (Figure 1e), which should be generated by the SiO$_2$ formation. The photograph and high-magnification images of bacteria cellulose/SiO$_2$ composites can verify this (Figure 1c,d). More interestingly, the original bacteria cellulose fibers with diameter 400 nm was decreased to 30 nm (Figure 1f). The small nanofibers were most possibly free from the aggregated cellulose fibers by alkaline treatment. Moreover, the SiO$_2$ formation within the gap or pores in the aggregated fiber bundles would also produce small nanofibers.
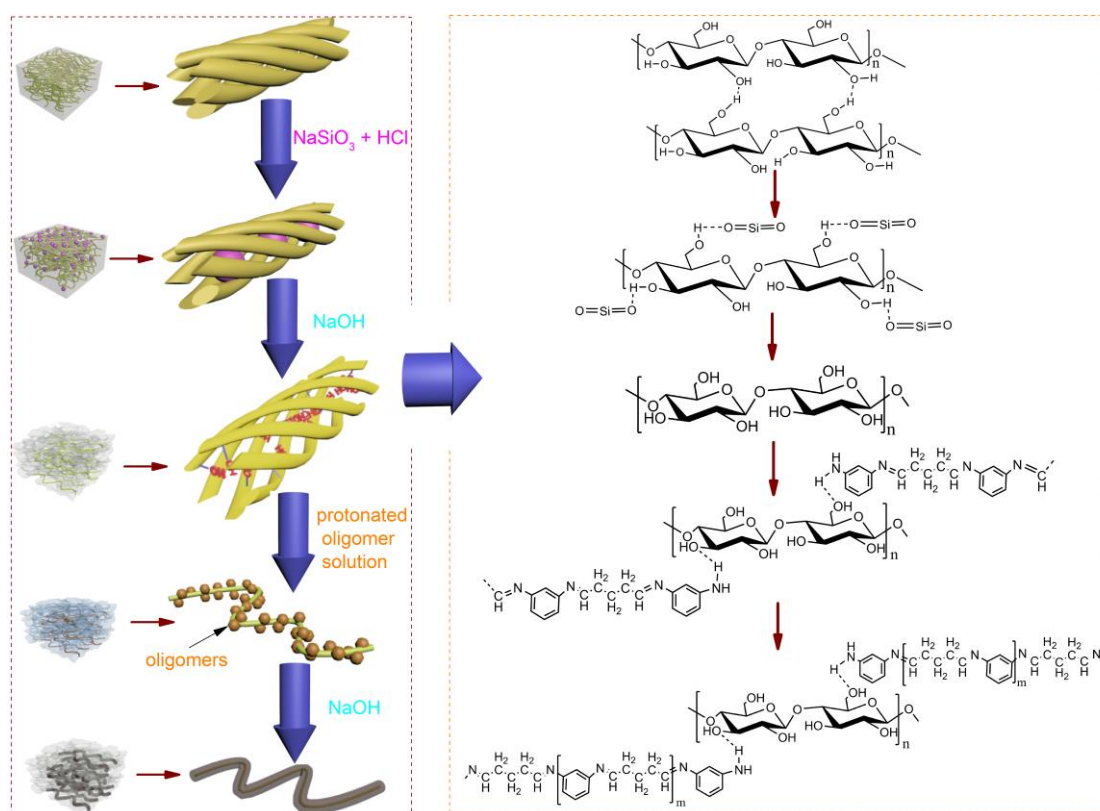
Scheme 1. The pathway of porous bacteria cellulose/poly Schiff base fabrication.
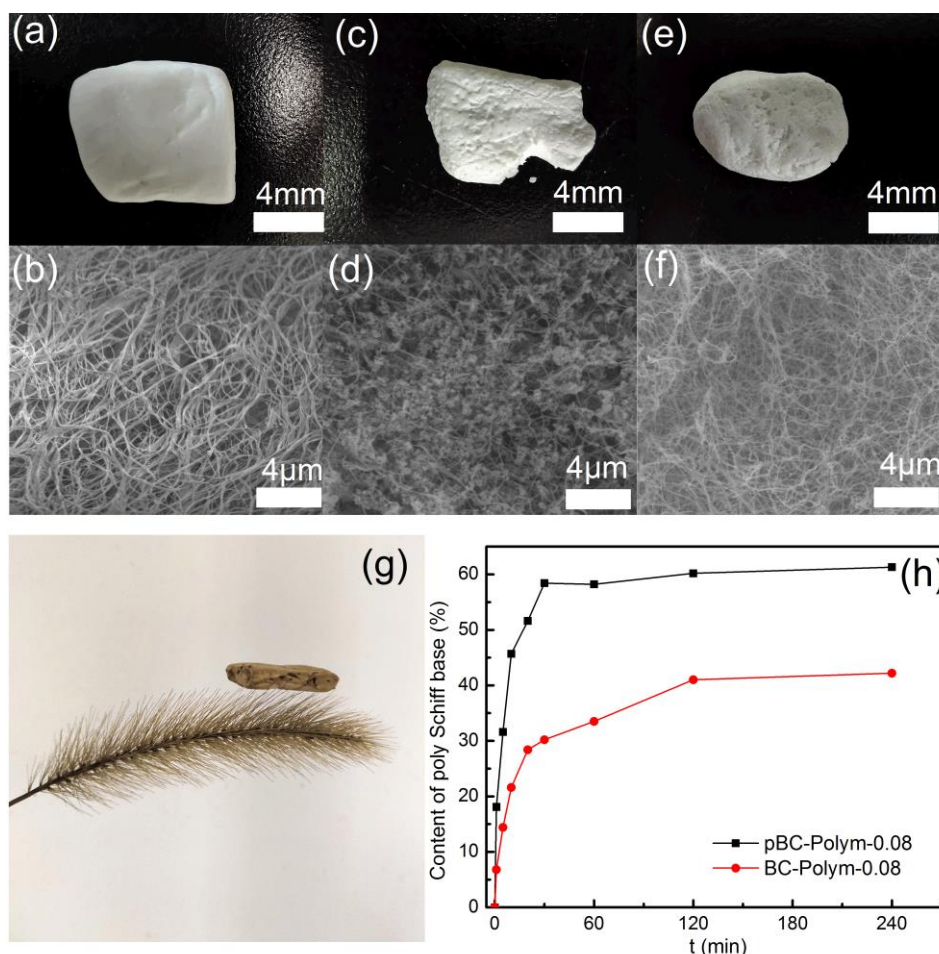
Figure 1. The photograph and of SEM images of bacteria cellulose (**a**,**b**), bacteria cellulose/SiO$_2$ (**c**,**d**) and pBC (**e**,**f**); the photograph of adsorbent with ultra-low density (**g**) and the content of poly Schiff base in pBC-Polym-0.08 and BC-Polym-0.08 with various reaction time (**h**).

XRD was used to validate the variation of bacteria cellulose before and after pretreatment. As seen in Figure 2a, the raw bacteria cellulose exhibited characteristic of typical cellulose I by diffraction peaks at 14.3° and 22.6° [30–32]. Noticeably, after the pretreatment, the peak intensity at 14.3° and 22.6° attenuated obviously, which indicated the decrease of crystallinity. On the other hand, the relative intensity of 16.4° increases. Moreover, a small peak located at 20.0° appeared, indexed as the (110) of cellulose II. It inferred that the structure of semi-crystalline region and amorphous region was altered via pretreatment. This can be explained by the separation of small cellulose nanofibers from original fiber bundles, which inevitably exposed new facet. It must be mentioned that in the raw cellulose the H bonding (by –OH) pushed the formation of cellulose crystal. The decrease of crystallinity of bacteria cellulose demonstrated the breaking of H bonding, which signified that the –OH is free from the crystal. This is conducive to increasing its affinity toward aqueous solution, which can promote the mass transfer within the body of bacteria cellulose.
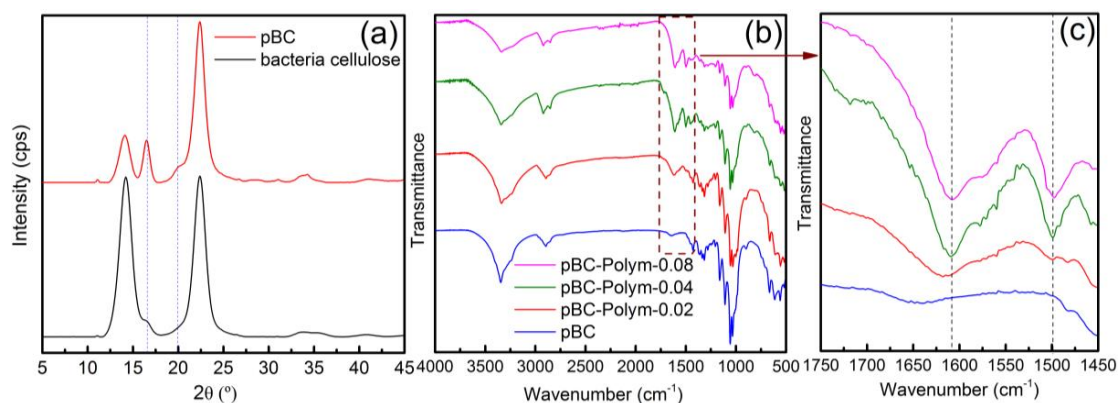
Figure 2. (**a**) XRD patterns of raw bacteria cellulose and pretreated bacteria cellulose. (**b**) FTIR spectra of pBC, pBC-Polym-0.02, pBC-Polym-0.04 and pBC-Polym-0.08 and (**c**) magnified graph in the range of 1750 to 1450 cm^{-1}.

3.2. Schiff Base Loading in Bacteria Cellulose

To allow the precursor coat onto the nanofibers, the bacteria cellulose firstly interacted with acidic aqueous mixture of *m*-phenylenediamine and glutaraldehyde. The pretreated bacteria cellulose immersed into precursor solution as soon as their contact. In contrast, the raw bacteria cellulose took ~30 min to be absolutely wetted by the solution. That should be caused by the pretreatment of bacteria cellulose, which alters its surface properties. After the saturation of precursor, the cellulose was put into the alkaline solution to speed up the polymerization process. Due to the strong interaction between –NH$_2$ and –OH, the poly Schiff base would stably coat onto the nanofibers of bacteria cellulose. The white cellulose became brown after the polymer coating (Figure 1g), which had ultra-low density. The final product was named as pBC-Polym-*x*, where pBC is the pretreated bacteria cellulose and *x* is the concentration of m-phenylenediamine in precursor solution. For comparison, the product without pretreatment was denoted as BC-Polym-*x*.

More importantly, the difference on the wettability of raw and pretreated bacteria cellulose changed the loading mass of poly Schiff base. As shown in Figure 1h, the polymer loading on pretreated bacteria cellulose increased very fast and it took 30 min for saturation. However, for the raw bacteria cellulose, it spent ~120 min for the complete loading. Typically, the content of poly Schiff base on pBC was at least 20% higher than that on raw materials, which can be vividly distinguished by the color of the product (Supplementary Section S2). This should be related to the improvement of the wettability of bacteria cellulose by the pretreatment.

3.3. Characterization

The ATR-FTIR technique was applied to study the structural variation of pBC before and after polymer coating. As seen in Figure 2b and c, functional groups including –OH (3343 cm^{-1}), C–H (2902 cm^{-1}), and –C–O–C– (1109 and 1164 cm^{-1}) can be found in the bare pBC [33–35]. After the polymer coating, two absorption bands at 1609 and 1493 cm^{-1} emerged. These corresponded to the stretching vibration of C=N and N–H shearing vibration in benzenoid amine structure [36,37]. Moreover, these two signals became obvious with the increase of polymer amount coating on the nanofibers.

The morphology of the final product was examined by the SEM technique, taking pBC-Polym-0.04 as an example. The morphology of the surface section was shown in Figure 3a that the gap between the nanofibers was filled with polymer. The result was identical for the cross-section of the product (Figure 3b). That is to say, the poly Schiff base uniformly coated on the nanofibers within the body of bacteria cellulose. The TEM images are given in Figure 3c (agglomeration) and 3d (single fiber). As shown, the incorporated thick polymer evolved to sheath-like structure to encapsulate the cellulose nanofibers, which was consistent with the SEM results. For pBC-Polym-0.02, only nanoparticles can be found on the nanofibers (Supplementary Figure S2). On the other hand,

pBC-Polym-0.08 showed a similar morphology but a higher density of coating (Supplementary Figure S3). The N_2 adsorption-desorption isotherm and porosity are shown in Supplementary Section S4, which indicated that the products were mainly composed of mesopores and macropores. In addition, the product exhibited good thermal stability (Supplementary Section S5), and this was beneficial for its practical applications.
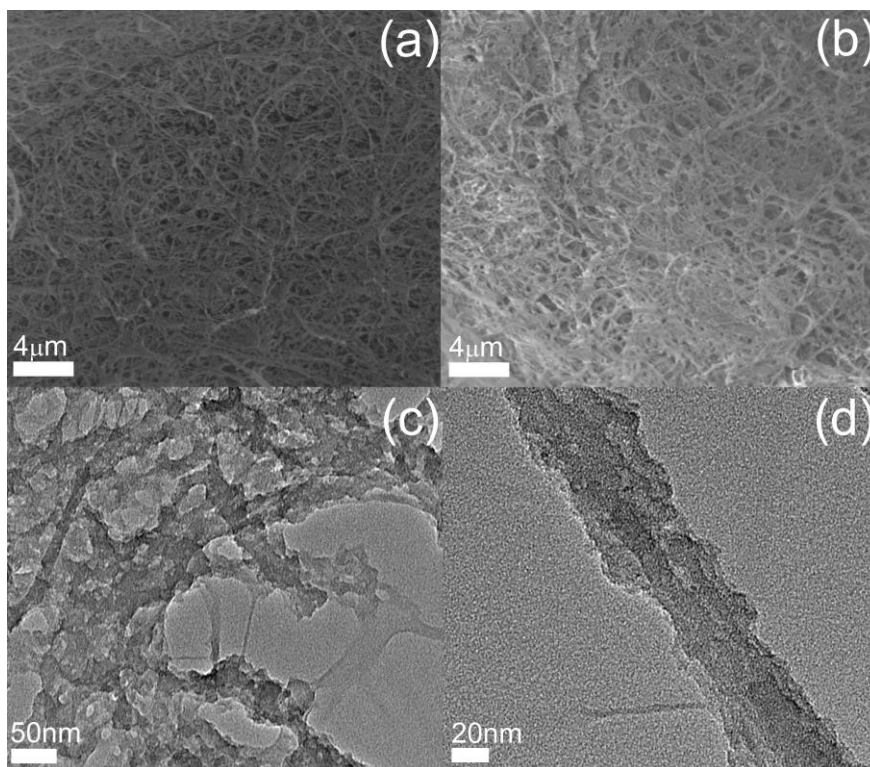

Figure 3. The SEM images of pBC-Polym-0.04: surface (**a**) and cross-section (**b**), and the TEM images of pBC-Polym-0.04: agglomerated fibers (**c**) and single fiber (**d**).

3.4. Adsorption Performance

The effect of pH on the adsorption was investigated and the results were given in Supplementary Section S6. As shown, the optimum pH for adsorption was ~2, which was related to the balance between protonation of the polymer and speciation of Cr ions at different pH. In the following experiments, pH will be used without special caution.

3.4.1. Adsorption Isotherm

Effect of initial concentration of Cr(VI) (100~500 mg L^{-1}) on the adsorption was investigated. As shown in Figure 4a, the adsorption capacity of the series of pBC-Polym-*x* rapidly increased with the rise of Cr(VI) concentration. Then, the adsorption process tended to be saturated. Similar trend was found for the samples without pretreatment (Figure 4b). However, the adsorption performance is much better for pBC-Polym-*x*. This can be ascribed to the high polymer loading and the high affinity to aqueous solution of pBC. On the other hand, the saturated capacity of pBC-Polym-0.04 was very close to that of pBC-Polym-0.08. The possible reason was that the thicker polymer coating on the nanofibers (pBC-Polym-0.08) decreased the utilization efficiency of the active materials.
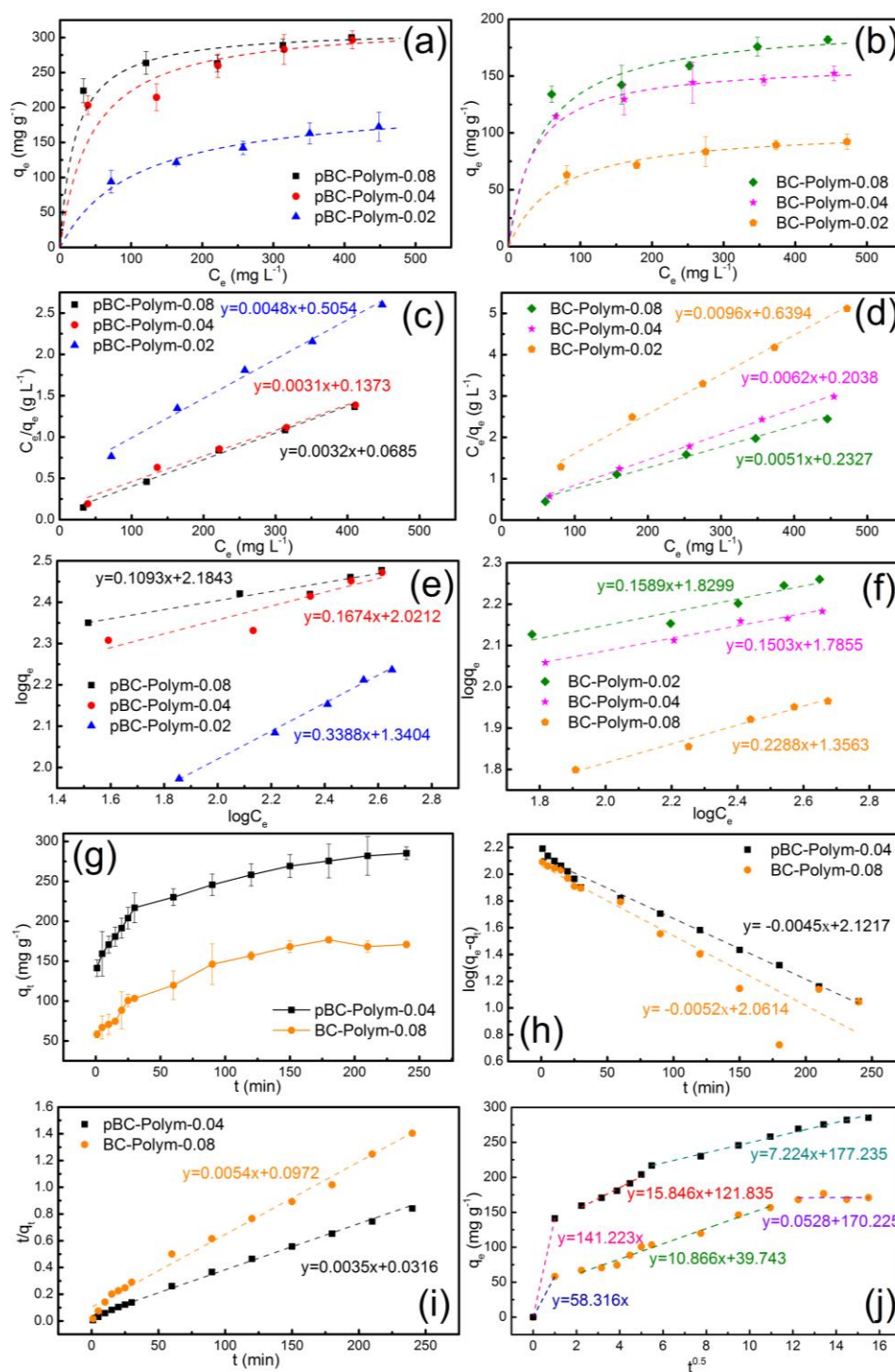
Figure 4. (**a**) Cr(VI) adsorption isotherms of pBC-Polym-0.02, pBC-Polym-0.04 and pBC-Polym-0.08, and (**b**) BC-Polym-0.02, BC-Polym-0.04 and BC-Polym-0.08. Their corresponding fitted Langmuir (**c**,**d**) and Freundlich isotherms (**e**,**f**). Effect of contact time on Cr(VI) adsorption (**g**) and kinetics modeling: (**h**) pseudo-first-order kinetic plots, (**i**) pseudo-second-order kinetic plots and (**j**) plots of intra particle model.

Furthermore, the experimental data (Figure 4c~f) were simulated by Langmuir and Freundlich models. The Langmuir and Freundlich equations are shown below:

$$\frac{C_e}{q_e} = \frac{C_e}{q_m} + \frac{1}{bq_m} \tag{5}$$

$$\log q_e = \log K_f + \frac{1}{n} \log C_e \tag{6}$$

where C_e is the Cr(VI) concentration at equilibrium, q_e is the adsorption capacity at equilibrium, q_m is the maximum adsorption capacity at saturation, b is the isotherm constant for Langmuir model, K_f and n are the constants of isotherm equation. The parameters were listed in Table 1.

Table 1. Isotherms parameter of Cr(VI) adsorption on pBC-Polym-x and BC-Polym-x samples.

Samples	Langmuir Isotherm			Freundlich Isotherm		
	q_{max} (mg g^{-1})	b (L mg^{-1})	R_L^2	K_f (mg g^{-1} (L mg^{-1})$^{1/n}$)	$1/n$	R_f^2
pBC-Polym-0.08	312.5	0.0467	0.995	152.848	0.1093	0.7374
pBC-Polym-0.04	321.5	0.0227	0.986	104.993	0.1674	0.7321
pBC-Polym-0.02	210.1	0.0094	0.991	21.901	0.3388	0.8990
BC-Polym-0.08	197.2	0.0218	0.991	67.590	0.1589	0.9083
BC-Polym-0.04	161.8	0.0303	0.999	61.018	0.1503	0.9830
BC-Polym-0.02	104.6	0.0151	0.995	22.716	0.2288	0.9795

Based on the calculation, adsorption behavior can be better described by the Langmuir model. This demonstrated a homogenous monolayer adsorption on poly Schiff base-coated cellulose nanofibers. The maximum adsorption capacity of pBC-Polym-0.04 was 321.5 mg g^{-1}. Remarkably, the adsorption capacity in this research was higher than most of the macroscopic adsorbents in previous studies (Table 2).

Table 2. Comparison pBC-Polym-0.04 with other macroscopic adsorbents.

Materials	Optimum pH	Kinetics	Adsorption Capacity (mg g^{-1})	Ref
Mesoporous carbon sponge	2~4	Pseudo-second-model	93.9	[38]
Polydopamine and Chitosan cross-linked graphene oxide	3	Pseudo-second-model	312.0	[39]
Magnetic graphene oxide foam	2	Pseudo-second-model	258.6	[40]
3D porous graphene oxide-maize amylopectin composites	5	Pseudo-second-model	13.6	[41]
3D porous cellulose	3	Pseudo second model	220.6	[42]
3D graphene oxide-NiFe LDH composite	3	Pseudo second model	53.6	[43]
Cyclodextrin functionalized 3D-graphene	2	Pseudo second model	107	[44]
Tetraethylenepentamine crosslinked chitosan oligosaccharide hydrogel	3	Pseudo second model	148.1	[45]
Polyaniline-coated bacterial cellulose mat	2	Pseudo second model	128	[26]
pBC-Polym-0.04	2	Pseudo second model	321.5	This study

3.4.2. Adsorption Kinetics

As shown in Figure 4g~i, the adsorption process of pBC-Polym-0.04 was very fast in the initial stage (≤30 min), involving 76% of the total capacity. This was presumably due to the physical adsorption. In this step, the negative charged Cr(VI) was adhered to positive charged adsorbent by electrostatic attraction. Additionally, the fast adsorption process was related to the high affinity to aqueous solution of the pBC-Polym-*x*, which promised effective mass transfer. The subsequently accumulative adsorption of Cr(VI) ultimately reached the equilibrium within 3 h. The pseudo-first and pseudo-second order models were adopted to analyze the adsorption process. As seen in Table 3, the pseudo-second-order model with the correlation coefficient (R^2) > 0.99 indicated that the Cr(VI)

adsorption was mainly controlled by chemical sorption. The adsorption process was deduced as the electrostatic attraction and redox-chelation. The Cr(VI) adsorption was initiated by electrostatic interaction. The Cr(VI) binding on surface of adsorbent was reduced to Cr(III) and chelated by quinoid imine group - the oxidation product of benzenoid amine structure [37,46]. The elaborate verification of adsorption mechanism was stated in Supplementary Section S7.

Table 3. The kinetics parameter of Cr(VI) adsorption on pBC-Polym-0.04 and BC-Polym-0.08.

Samples	q_{exp}	Pseudo-First-Order Model $\log(q_e-q_t)=\log q_e-\frac{k_1}{2.303}t$			Pseudo-Second-Order Model $\frac{t}{q_t}=\frac{1}{k_2 q_e^2}+\frac{1}{q_e}t$			Intra Particles Diffusion $q_t=k_i t^{0.5}+C$					
		q_e	k_1	R^2	q_e	k_2	R^2	k_{id1}	C_1	k_{id2}	C_2	k_{id3}	C_3
pBC-Polym-0.04	285.2	132.3	0.010	0.9903	289.8	0.11	0.9971	141.2	0	15.8	121.8	7.2	177.2
BC-Polym-0.08	170.9	115.1	0.012	0.8993	183.8	0.056	0.9915	58.3	0	10.8	39.7	0.052	170.2

Furthermore, the Weber–Morris intraparticle diffusion model was used to describe the adsorption process (Figure 4j). The whole adsorption can be divided into three regions: (1) Cr(VI) diffusion in aqueous solution onto the exterior surface of adsorbent; (2) Cr(VI) permeation into the inner section of adsorbent and Cr(VI) diffusion into the internal polymers; (3) chemical sorption and reaching equilibrium. Clearly, the surface diffusion of pBC-Polym-0.04 completed within 1 minute. From 0~1 min, Cr(VI) was instantly captured by the poly Schiff base deposited on the surface of aerogel. In the second procedure, faster permeation and mass transfer of pBC-Polym-0.04 was observed. For BC-Polym-0.04, ascribed to the weaker affinity toward solution, the permeation and adsorption of inner polymers lasted from 5~120 min. The k_{id} listed in Table 3 manifested the high adsorption rate of pBC-Polym-0.04.

3.4.3. Dynamic Adsorption

The fast adsorption process is vividly illustrated in Figure 5a. A piece of pBC-Polym-0.04 was directly immersed into the Cr(VI) solution and it was taken out after 2 s. The liquid was squeezed out that the clean water was obtained. Considering this superior property, the pBC-Polym was filled in a column to achieve flow-through adsorption. The practical image is shown in Figure 5b. Here, 25 mL of Cr(VI) solution was pumped to the column by peristaltic pump to flow through the macroscopic adsorbent with a constant velocity.

In the flow-through adsorption, effect of concentration was examined firstly. The flow velocity was set as 28.4 μL min^{-1}. As shown in Figure 6a, the removal rate was persistently remained at above 96% when Cr(VI) concentration < 100 mg L^{-1}. This indicated the excellent performance of pBC-Polym in dynamic process. Figure 6b revealed the relationship between influent velocity and removal efficiency in dynamic adsorption (C_0 = 50 mg L^{-1}). The removal rate hardly decreases with the increased flow rate. This sufficiently demonstrated the high mass transfer efficiency of the ions within the body of adsorbent and strongly verified the high prospect of pBC-Polym in wastewater purification. Moreover, the adsorbent exhibited excellent ability in the treatment of diverse metal ions and organic dyes (Supplementary Section S8).
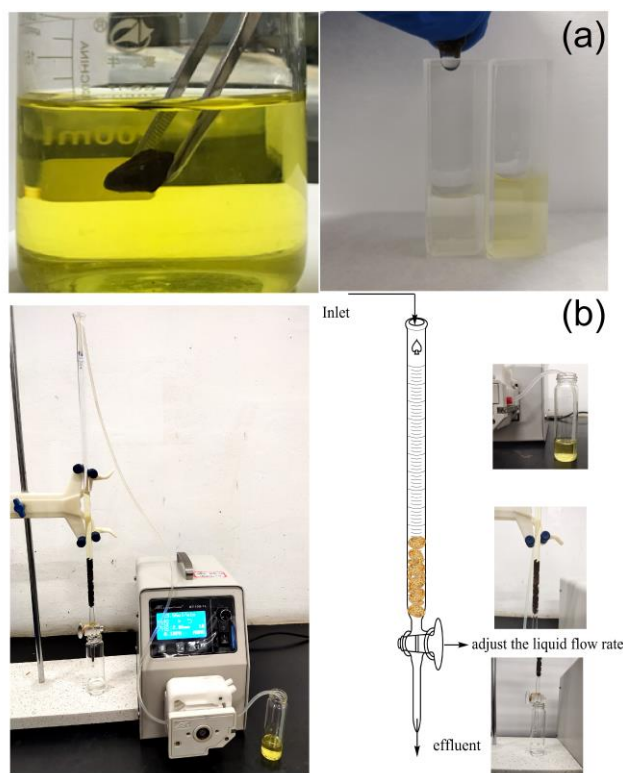
Figure 5. (**a**) Illustration on the fast and convenient adsorption by pBC-Polym-0.04, and (**b**) experimental apparatus for dynamic adsorption.
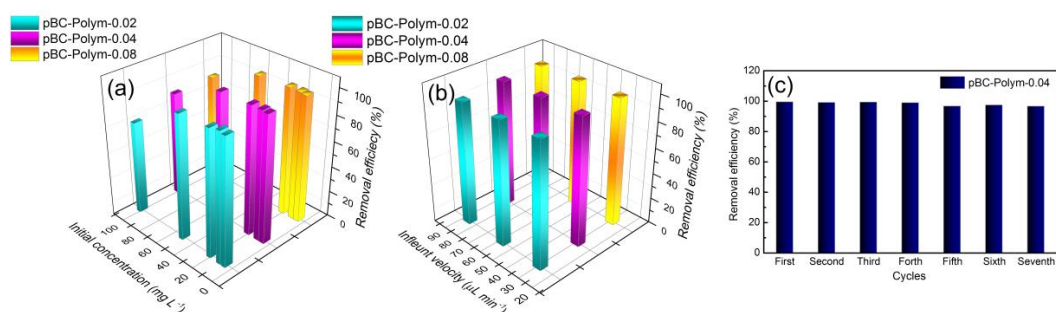

Figure 6. Effect of initial Cr(VI) concentration (**a**) and effect of velocity (**b**) on dynamic adsorption by pBC-Polym-0.02, pBC-Polym-0.04 and pBC-Polym-0.08; recycling behavior of the pBC-Polym-0.04 in Cr(VI) adsorption (**c**).

3.4.4. Recyclability

The repeated adsorption was tested by dynamic adsorption using 25 mL of 20 mg L^{-1} Cr(VI) solution as simulated effluent. 100 mL of 2M NaOH was applied as desorption solution and flow through the adsorbent in the column. The adsorbent was rinsed and freeze-dried after desorption for next cycle. The Cr(VI) removal rate of each cycle was shown in Figure 6c. For seven cycles, no obvious performance attenuation was observed. Typically, the Cr(VI) removal rate of adsorbent remained 96.5%, implying its distinguished reusability.

4. Conclusion

We have successfully fabricated the poly Schiff base-coated bacteria cellulose without the conventional dispersion treatment of the cellulose aerogel. The key is to pretreat the bacteria cellulose with sodium silicate to exfoliate the nanofibers from the big bundles of raw cellulose fibers.

Due to the intact texture of the pretreated bacteria cellulose, the composite aerogel is of good properties (e.g., mechanical and thermal) and high mass transfer efficiency. The adsorption capacity of the aerogel is 321.5 (Cr(VI)), 256.4 (Cu(II)), 153.8 (Re(VII)), 333.3 (Conga red), and 370.3 (Orange G) mg g^{-1}. The adsorption process obeys the pseudo-second order kinetic. The adsorbent can be regenerated easily and used to remove the pollutants without obvious performance attenuation.

Supplementary Materials: The following are available online at http://www.mdpi.com/2073-4360/12/3/714/s1, 1. Detail of Fabrication, 2. Photograph of pBC-Polym-0.04 and BC-Polym-0.04, 3. The morphology of pBC-Polym-0.02 and pBC-Polym-0.08, 4. Specific surface area and porosity, 5. Thermal stability, 7. Adsorption mechanism, 8. Other pollutants

Author Contributions: Conceptualization, L.R. and L.Z.; methodology, L.R.; software, L.R.; validation, Z.Y., and H.W.; formal analysis, L.R; investigation, L.H.; resources, Y.H.; data curation, L.H.; writing—original draft preparation, L.R.; writing—review and editing, L.Z.; visualization, Z.Y.; supervision, H.W.; project administration, Z.Y.; funding acquisition, H.W. All authors have read and agreed to the published version of the manuscript.

Conflicts of Interest: The authors all declare that they have no conflict of interest.

References

1.　Hausladen, D.M.; Alexander-Ozinskas, A.; McClain, C.; Fendorf, S. Hexavalent Chromium Sources and Distribution in California Groundwater. *Environ. Sci. Technol.* **2018**, *52*, 8242–8251. [CrossRef]

2.　Lin, X.; Sun, Z.; Zhao, L.; Ma, J.; Li, X.; He, F.; Hou, H. Toxicity of Exogenous Hexavalent Chromium to Soil-Dwelling Springtail Folsomia Candida in Relation to Soil Properties and Aging Time. *Chemosphere* **2019**, *224*, 734–742. [CrossRef]

3.　Yan, X.; Song, M.; Zhou, M.; Ding, C.; Wang, Z.; Wang, Y.; Yang, W.; Yang, Z.; Liao, Q.; Shi, Y. Response of Cupriavidus Basilensis B-8 to Cuo Nanoparticles Enhances Cr(Vi) Reduction. *Sci. Total Environ.* **2019**, *688*, 46–55. [CrossRef] [PubMed]

4.　Tran, H.N.; Nguyen, D.T.; Le, G.T.; Tomul, F.; Lima, E.C.; Woo, S.H.; Sarmah, A.K.; Nguyen, H.Q.; Nguyen, P.T.; Nguyen, D.D.; et al. Adsorption Mechanism of Hexavalent Chromium onto Layered Double Hydroxides-Based Adsorbents: A Systematic in-Depth Review. *J. Hazard Mater.* **2019**, *373*, 258–270. [CrossRef] [PubMed]

5.　Kalidhasan, S.; Kumar, A.S.K.; Rajesh, V.; Rajesh, N. The Journey Traversed in the Remediation of Hexavalent Chromium and the Road Ahead toward Greener Alternatives—a Perspective. *Coord. Chem. Rev.* **2016**, *317*, 157–166. [CrossRef]

6.　Wang, T.; Zhang, L.; Li, C.; Yang, W.; Song, T.; Tang, C.; Meng, Y.; Dai, S.; Wang, H.; Chai, L.; et al. Synthesis of Core-Shell Magnetic Fe3o4@Poly(M-Phenylenediamine) Particles for Chromium Reduction and Adsorption. *Environ. Sci. Technol.* **2015**, *49*, 5654–5662. [CrossRef]

7.　Liang, H.; Song, B.; Peng, P.; Jiao, G.; Yan, X.; She, D. Preparation of Three-Dimensional Honeycomb Carbon Materials and Their Adsorption of Cr(Vi). *Chem. Eng. J.* **2019**, *367*, 9–16. [CrossRef]

8.　Huang, M.-R.; Lu, H.-J.; Li, X.-G. Synthesis and Strong Heavy-Metal Ion Sorption of Copolymer Microparticles from Phenylenediamine and Its Sulfonate. *J. Mater. Chem.* **2012**, *22*, 34. [CrossRef]

9.　Wang, H.; Hou, L.; Shen, Y.; Huang, L.; He, Y.; Yang, W.; Yuan, T.; Jin, L.; Tang, C.J.; Zhang, L. Synthesis of Core-Shell Uio-66-Poly(M-Phenylenediamine) Composites for Removal of Hexavalent Chromium. *Environ Sci. Pollut. Res. Int.* **2020**, *27*, 4115–4126. [CrossRef]

10.　Wang, H.; He, Y.; Chai, L.; Lei, H.; Yang, W.; Hou, L.; Yuan, T.; Jin, L.; Tang, C.; Luo, J. Highly-Dispersed Fe2o3@C Electrode Materials for Pb2+ Removal by Capacitive Deionization. *Carbon* **2019**, *153*, 12–20. [CrossRef]

11.　Hemavathy, R.V.; Kumar, P.S.; Kanmani, K.; Jahnavi, N. Adsorptive Separation of Cu (Ii) Ions from Aqueous Medium Using Thermally/Chemically Treated Cassia Fistula Based Biochar. *J. Clean. Prod.* **2020**, *249*, 1–12. [CrossRef]

12. Luo, J.; Crittenden, J.C. Nanomaterial Adsorbent Design: From Bench Scale Tests to Engineering Design. *Environ. Sci. Technol.* **2019**, *53*, 10537–10538. [CrossRef] [PubMed]

13. Alfaro, I.; Molina, L.; González, P.; Gaete, J.; Valenzuela, F.; Marco, J.F.; Sáez, C.; Basualto, C. Silica-Coated Magnetite Nanoparticles Functionalized with Betaine and Their Use as an Adsorbent for Mo (Vi) and Re(Vii) Species from Acidic Aqueous Solutions. *J. Ind. Eng. Chem.* **2019**, *78*, 271–283. [CrossRef]

14. Du, Z.; Zheng, T.; Wang, P. Experimental and Modelling Studies on Fixed Bed Adsorption for Cu(Ii) Removal from Aqueous Solution by Carboxyl Modified Jute Fiber. *Powder Technol.* **2018**, *338*, 952–959. [CrossRef]

15. Wang, H.; Li, X.; Chai, L.; Zhang, L. Nano-Functionalized Filamentous Fungus Hyphae with Fast Reversible Macroscopic Assembly & Disassembly Features. *Chem. Commun.* **2015**, *51*, 8524–8527.

16. Wang, D. A Critical Review of Cellulose-Based Nanomaterials for Water Purification in Industrial Processes. *Cellulose* **2018**, *26*, 687–701. [CrossRef]

17. Luo, H.; Xie, J.; Wang, J.; Yao, F.; Yang, Z.; Wan, Y. Step-by-Step Self-Assembly of 2d Few-Layer Reduced Graphene Oxide into 3d Architecture of Bacterial Cellulose for a Robust, Ultralight, and Recyclable All-Carbon Absorbent. *Carbon* **2018**, *139*, 824–832. [CrossRef]

18. Hu, Y.; Liu, F.; Sun, Y.; Xu, X.; Chen, X.; Pan, B.; Sun, D.; Qian, J. Bacterial Cellulose Derived Paper-Like Purifier with Multifunctionality for Water Decontamination. *Chem. Eng. J.* **2019**, *371*, 730–737. [CrossRef]

19. Carpenter, A.W.; de Lannoy, C.F.; Wiesner, M.R. Cellulose Nanomaterials in Water Treatment Technologies. *Environ. Sci. Technol.* **2015**, *49*, 5277–5287. [CrossRef]

20. Cheng, R.; Kang, M.; Zhuang, S.; Shi, L.; Zheng, X.; Wang, J. Adsorption of Sr (Ii) from Water by Mercerized Bacterial Cellulose Membrane Modified with Edta. *J. Hazard Mater.* **2019**, *364*, 645–653. [CrossRef]

21. Hu, Y.; Chen, C.; Yang, L.; Cui, J.; Hao, Q.; Sun, D. Handy Purifier Based on Bacterial Cellulose and Ca-Montmorillonite Composites for Efficient Removal of Dyes and Antibiotics. *Carbohydr. Polym.* **2019**, *222*, 115017. [CrossRef] [PubMed]

22. Zhu, T.; Mao, J.; Cheng, Y.; Liu, H.; Lv, L.; Ge, M.; Li, S.; Huang, J.; Chen, Z.; Li, H.; et al. Recent Progress of Polysaccharide-Based Hydrogel Interfaces for Wound Healing and Tissue Engineering. *Adv. Mater. Interfaces* **2019**, *6*, 17. [CrossRef]

23. Mensah, A.; Lv, P.; Narh, C.; Huang, J.; Wang, D.; Wei, Q. Sequestration of Pb (Ii) Ions from Aqueous Systems with Novel Green Bacterial Cellulose Graphene Oxide Composite. *Materials* **2019**, *12*, 218. [CrossRef] [PubMed]

24. Jin, X.; Xiang, Z.; Liu, Q.; Chen, Y.; Lu, F. Polyethyleneimine-Bacterial Cellulose Bioadsorbent for Effective Removal of Copper and Lead Ions from Aqueous Solution. *Bioresour. Technol.* **2017**, *244*, 844–849. [CrossRef]

25. Wang, J.; Lu, X.; Ng, P.F.; Lee, K.I.; Fei, B.; Xin, J.H.; Wu, J.Y. Polyethylenimine Coated Bacterial Cellulose Nanofiber Membrane and Application as Adsorbent and Catalyst. *J. Colloid Interface Sci.* **2015**, *440*, 32–38. [CrossRef]

26. Jahan, K.; Kumar, N.; Verma, V. Removal of Hexavalent Chromium from Potable Drinking Using a Polyaniline-Coated Bacterial Cellulose Mat. *Environ. Sci. Water Res. Technol.* **2018**, *4*, 1589–1603. [CrossRef]

27. Yang, Z.; Ren, L.; Jin, L.; Huang, L.; He, Y.; Tang, J.; Yang, W.; Wang, H. In-Situ Functionalization of Poly(M-Phenylenediamine) Nanoparticles on Bacterial Cellulose for Chromium Removal. *Chem. Eng. J.* **2018**, *344*, 441–452. [CrossRef]

28. He, C.; Huang, J.; Li, S.; Meng, K.; Zhang, L.; Chen, Z.; Lai, Y. Mechanically Resistant and Sustainable Cellulose-Based Composite Aerogels with Excellent Flame Retardant, Sound-Absorption, and Superantiwetting Ability for Advanced Engineering Materials. *ACS Sustain. Chem. Eng.* **2017**, *6*, 927–936. [CrossRef]

29. Zhang, H.; Xu, X.; Chen, C.; Chen, X.; Huang, Y.; Sun, D. In Situ Controllable Fabrication of Porous Bacterial Cellulose. *Mater. Lett.* **2019**, *249*, 104–107. [CrossRef]

30. Yan, H.; Chen, X.; Song, H.; Li, J.; Feng, Y.; Shi, Z.; Wang, X.; Lin, Q. Synthesis of Bacterial Cellulose and Bacterial Cellulose Nanocrystals for Their Applications in the Stabilization of Olive Oil Pickering Emulsion. *Food Hydrocoll.* **2017**, *72*, 127–135. [CrossRef]

31. Stoica-Guzun, A.; Stroescu, M.; Jinga, S.I.; Mihalache, N.; Botez, A.; Matei, C.; Berger, D.; Damian, C.M.; Ionita, V. Box-Behnken Experimental Design for Chromium(Vi) Ions Removal by Bacterial Cellulose-Magnetite Composites. *Int. J. Biol. Macromol.* **2016**, *91*, 1062–1072. [CrossRef] [PubMed]

32. Urbina, L.; Guaresti, O.; Requies, J.; Gabilondo, N.; Eceiza, A.; Corcuera, M.A.; Retegi, A. Design of Reusable Novel Membranes Based on Bacterial Cellulose and Chitosan for the Filtration of Copper in Wastewaters. *Carbohydr. Polym.* **2018**, *193*, 362–372. [CrossRef] [PubMed]

33. Oh, S.Y.; Yoo, D.I.; Shin, Y.; Seo, G. Ftir Analysis of Cellulose Treated with Sodium Hydroxide and Carbon Dioxide. *Carbohydr. Res.* **2005**, *340*, 417–428. [CrossRef] [PubMed]

34. Chen, S.; Huang, Y. Bacterial Cellulose Nanofibers Decorated with Phthalocyanine: Preparation, Characterization and Dye Removal Performance. *Mater. Lett.* **2015**, *142*, 235–237. [CrossRef]

35. Jiang, J.; Zhu, J.; Zhang, Q.; Zhan, X.; Chen, F. A Shape Recovery Zwitterionic Bacterial Cellulose Aerogel with Superior Performances for Water Remediation. *Langmuir* **2019**, *35*, 11959–11967. [CrossRef] [PubMed]

36. Zhang, L.; Chai, L.; Liu, J.; Wang, H.; Yu, W.; Sang, P. Ph Manipulation: A Facile Method for Lowering Oxidation State and Keeping Good Yield of Poly (M-Phenylenediamine) and Its Powerful Ag+ Adsorption Ability. *Langmuir* **2011**, *27*, 13729–13738. [CrossRef]

37. Ren, L.; Yang, Z.; Jin, L.; Yang, W.; Shi, Y.; Wang, S.; Yi, H.; Wei, D.; Wang, H.; Zhang, L. Hydrothermal Synthesis of Chemically Stable Cross-Linked Poly-Schiff Base for Efficient Cr (Vi) Removal. *J. Mater. Sci.* **2019**, *55*, 3259–3278. [CrossRef]

38. Liu, Y.; Liu, S.; Li, Z.; Ma, M.; Wang, B. A Microwave Synthesized Mesoporous Carbon Sponge as an Efficient Adsorbent for Cr (Vi) Removal. *RSC Adv.* **2018**, *8*, 7892–7898. [CrossRef]

39. Li, L.; Wei, Z.; Liu, X.; Yang, Y.; Deng, C.; Yu, Z.; Guo, Z.; Shi, J.; Zhu, C.; Guo, W.; et al. Biomaterials Cross-Linked Graphene Oxide Composite Aerogel with a Macro–Nanoporous Network Structure for Efficient Cr (Vi) Removal. *Int. J. Biol. Macromol.* **2019**, (in press). [CrossRef]

40. Lei, Y.; Chen, F.; Luo, Y.; Zhang, L. Three-Dimensional Magnetic Graphene Oxide Foam/Fe3o4 Nanocomposite as an Efficient Absorbent for Cr (Vi) Removal. *J. Mater. Sci.* **2014**, *49*, 4236–4245. [CrossRef]

41. Zhao, X.; Xu, X.; Teng, J.; Zhou, N.; Zhou, Z.; Jiang, X.; Jiao, F.; Yu, J. Three-Dimensional Porous Graphene Oxide-Maize Amylopectin Composites with Controllable Pore-Sizes and Good Adsorption-Desorption Properties: Facile Fabrication and Reutilization, and the Adsorption Mechanism. *Ecotoxicol. Environ. Saf.* **2019**, *176*, 11–19. [CrossRef] [PubMed]

42. Liu, L.; Liao, Q.; Xie, J.; Qian, Z.; Zhu, W.; Chen, X.; Su, X.; Meng, R.; Yao, J. Synthetic Control of Three-Dimensional Porous Cellulose-Based Bioadsorbents: Correlation between Structural Feature and Metal Ion Removal Capability. *Cellulose* **2016**, *23*, 3819–3835. [CrossRef]

43. Zheng, Y.; Cheng, B.; You, W.; Yu, J.; Ho, W. 3D Hierarchical Graphene Oxide-Nife Ldh Composite with Enhanced Adsorption Affinity to Congo Red, Methyl Orange and Cr (Vi) Ions. *J. Hazard Mater.* **2019**, *369*, 214–225. [CrossRef] [PubMed]

44. Wang, Z.; Lin, F.; Huang, L.; Chang, Z.; Yang, B.; Liu, S.; Zheng, M.; Lu, Y.; Chen, J. Cyclodextrin Functionalized 3d-Graphene for the Removal of Cr (Vi) with the Easy and Rapid Separation Strategy. *Environ. Pollut.* **2019**, *254*, 112854. [CrossRef]

45. Kim, M.K.; Sundaram, K.S.; Iyengar, G.A.; Lee, K.-P. A Novel Chitosan Functional Gel Included with Multiwall Carbon Nanotube and Substituted Polyaniline as Adsorbent for Efficient Removal of Chromium Ion. *Chem. Eng. J.* **2015**, *267*, 51–64. [CrossRef]

46. Cheng, Z.; Dai, Z.; Li, J.; Wang, H.; Huang, M.-R.; Li, X.-G.; Liao, Y. Template-Free Synthesis of Tunable Hollow Microspheres of Aniline and Aminocarbazole Copolymers Emitting Colorful Fluorescence for Ultrasensitive Sensors. *Chem. Eng. J.* **2019**, *357*, 776–786. [CrossRef]